Simultaneous measurement of temperature and refractive index using focused ion beam milled Fabry-Perot cavities in optical fiber micro-tips

Ricardo M. André,[1,2,*] Stephen C. Warren-Smith,[2] Martin Becker,[2] Jan Dellith,[2] Manfred Rothhardt,[2] M. I. Zibaii,[3] H. Latifi,[3] Manuel B. Marques,[1] Hartmut Bartelt,[2] and Orlando Frazão[1]

[1]*INESC TEC and Department of Physics and Astronomy, Faculty of Sciences, University of Porto, Rua do Campo Alegre 687, 4150-179 Porto, Portugal*
[2]*Leibniz Institute of Photonic Technology (IPHT Jena), Albert-Einstein-Straße 9, 07745 Jena, Germany*
[3]*Laser and Plasma Research Institute, Shahid Beheshti University, Evin, Tehran, Iran*
[*]*rmeloandre@fc.up.pt*

Abstract: Optical fiber micro-tips are promising devices for sensing applications in small volume and difficult to access locations, such as biological and biomedical settings. The tapered fiber tips are prepared by dynamic chemical etching, reducing the size from 125 μm to just a few μm. Focused ion beam milling is then used to create cavity structures on the tapered fiber tips. Two different Fabry-Perot micro-cavities have been prepared and characterized: a solid silica cavity created by milling two thin slots and a gap cavity. A third multi-cavity structure is fabricated by combining the concepts of solid silica cavity and gap cavity. This micro-tip structure is analyzed using a fast Fourier transform method to demultiplex the signals of each cavity. Simultaneous measurement of temperature and external refractive index is then demonstrated, presenting sensitivities of -15.8 pm/K and −1316 nm/RIU, respectively.

OCIS codes: (050.2230) Fabry-Perot; (060.4005) Microstructured fibers; (230.4000) Microstructure fabrication.

References and links

1. J. L. Santos and F. Farahi, *Handbook of Optical Sensors* (CRC Press, 2014).
2. R. A. Potyrailo, S. E. Hobbs, and G. M. Hieftje, "Optical waveguide sensors in analytical chemistry: today's instrumentation, applications and trends for future development," Fresenius J. Anal. Chem. **362**(4), 349–373 (1998).
3. F. C. Favero, L. Araujo, G. Bouwmans, V. Finazzi, J. Villatoro, and V. Pruneri, "Spheroidal Fabry-Perot microcavities in optical fibers for high-sensitivity sensing," Opt. Express **20**(7), 7112–7118 (2012).
4. Y. Wang, D. N. Wang, C. Wang, and T. Hu, "Compressible fiber optic micro-Fabry-Pérot cavity with ultra-high pressure sensitivity," Opt. Express **21**(12), 14084–14089 (2013).
5. T. Valis, D. Hogg, and R. M. Measures, "Fiber optic Fabry-Perot strain gauge," IEEE Photonics Technol. Lett. **2**(3), 227–228 (1990).
6. C. E. Lee, W. N. Gibler, R. A. Atkins, and H. F. Taylor, "In-line fiber Fabry-Perot interferometer with high-reflectance internal mirrors," J. Lightwave Technol. **10**(10), 1376–1379 (1992).
7. Y. Zhang, H. Shibru, K. L. Cooper, and A. Wang, "Miniature fiber-optic multicavity Fabry-Perot interferometric biosensor," Opt. Lett. **30**(9), 1021–1023 (2005).
8. Y. Rao, B. Xu, Z.-L. Ran, and Y. Gong, "Micro extrinsic fiber-optic Fabry-Perot interferometric sensor based on erbium- and boron- doped fibers," Chin. Phys. Lett. **25**, 024208 (2010).
9. P. Betts, "Bragg grating Fabry-Perot interferometer with variable finesse," Opt. Eng. **43**(5), 1258–1259 (2004).
10. P. Domachuk, I. C. M. Littler, M. Cronin-Golomb, and B. J. Eggleton, "Compact resonant integrated microfluidic refractometer," Appl. Phys. Lett. **88**(9), 093513 (2006).
11. T. Wei, Y. Han, H.-L. Tsai, and H. Xiao, "Miniaturized fiber inline Fabry-Perot interferometer fabricated with a femtosecond laser," Opt. Lett. **33**(6), 536–538 (2008).
12. T. Wei, Y. Han, Y. Li, H.-L. Tsai, and H. Xiao, "Temperature-insensitive miniaturized fiber inline Fabry-Perot interferometer for highly sensitive refractive index measurement," Opt. Express **16**(8), 5764–5769 (2008).

#261196 Received 17 Mar 2016; revised 12 Jun 2016; accepted 12 Jun 2016; published 15 Jun 2016

13. Z. L. Ran, Y. J. Rao, W. J. Liu, X. Liao, and K. S. Chiang, "Laser-micromachined Fabry-Perot optical fiber tip sensor for high-resolution temperature-independent measurement of refractive index," Opt. Express **16**(3), 2252–2263 (2008).
14. C. R. Liao, T. Y. Hu, and D. N. Wang, "Optical fiber Fabry-Perot interferometer cavity fabricated by femtosecond laser micromachining and fusion splicing for refractive index sensing," Opt. Express **20**(20), 22813–22818 (2012).
15. L. Yuan, T. Wei, Q. Han, H. Wang, J. Huang, L. Jiang, and H. Xiao, "Fiber inline Michelson interferometer fabricated by a femtosecond laser," Opt. Lett. **37**(21), 4489–4491 (2012).
16. A. A. Said, M. Dugan, S. de Man, and D. Iannuzzi, "Carving fiber-top cantilevers with femtosecond laser micromachining," J. Micromech. Microeng. **18**(3), 035005 (2008).
17. D. N. Wang, "Micro-engineered optical fiber sensors fabricated by femtosecond laser micromachining," in *Imaging and Applied Optics Technical Digest* (Optical Society of America, 2012).
18. J. L. Kou, J. Feng, L. Ye, F. Xu, and Y. Q. Lu, "Miniaturized fiber taper reflective interferometer for high temperature measurement," Opt. Express **18**(13), 14245–14250 (2010).
19. W. Yuan, F. Wang, A. Savenko, D. H. Petersen, and O. Bang, "Note: Optical fiber milled by focused ion beam and its application for Fabry-Pérot refractive index sensor," Rev. Sci. Instrum. **82**(7), 076103 (2011).
20. R. M. André, S. Pevec, M. Becker, J. Dellith, M. Rothhardt, M. B. Marques, D. Donlagic, H. Bartelt, and O. Frazão, "Focused ion beam post-processing of optical fiber Fabry-Perot cavities for sensing applications," Opt. Express **22**(11), 13102–13108 (2014).
21. T. Wieduwilt, J. Dellith, F. Talkenberg, H. Bartelt, and M. A. Schmidt, "Reflectivity enhanced refractive index sensor based on a fiber-integrated Fabry-Perot microresonator," Opt. Express **22**(21), 25333–25346 (2014).
22. L. V. Nguyen, M. Vasiliev, and K. Alameh, "Three-wave fiber Fabry–Perot interferometer for simultaneous measurement of temperature and water salinity of seawater," IEEE Photonics Technol. Lett. **23**(7), 450–452 (2011).
23. J. L. Kou, J. Feng, Q. J. Wang, F. Xu, and Y. Q. Lu, "Microfiber-probe-based ultrasmall interferometric sensor," Opt. Lett. **35**(13), 2308–2310 (2010).
24. S. C. Warren-Smith, R. M. André, C. Perrella, J. Dellith, H. Bartelt, and H. Bartelt, "Direct core structuring of microstructured optical fibers using focused ion beam milling," Opt. Express **24**(1), 378–387 (2016).
25. A. Iadicicco, S. Campopiano, A. Cutolo, M. Giordano, and A. Cusano, "Self temperature referenced refractive index sensor by non-uniform thinned fiber Bragg gratings," Sens. Actuators B Chem. **120**(1), 231–237 (2006).
26. D. A. Pereira, "Fiber Bragg grating sensing system for simultaneous measurement of salinity and temperature," Opt. Eng. **43**(2), 299–304 (2004).
27. A. P. Zhang, Li-Yang Shao, Jin-Fei Ding, and Sailing He, "Sandwiched long-period gratings for simultaneous measurement of refractive index and temperature," IEEE Photonics Technol. Lett. **17**(11), 2397–2399 (2005).
28. X. Chen, K. Zhou, L. Zhang, and I. Bennion, "Simultaneous measurement of temperature and external refractive index by use of a hybrid grating in D fiber with enhanced sensitivity by HF etching," Appl. Opt. **44**(2), 178–182 (2005).
29. P. Lu, L. Men, K. Sooley, and Q. Chen, "Tapered fiber Mach–Zehnder interferometer for simultaneous measurement of refractive index and temperature," Appl. Phys. Lett. **94**(13), 131110 (2009).
30. T. Wang and M. Wang, "Fabry–Pérot fiber sensor for simultaneous measurement of refractive index and temperature based on an in-fiber ellipsoidal cavity," IEEE Photonics Technol. Lett. **24**(19), 1733–1736 (2012).
31. A. N. Bashkatov and E. A. Genina, "Water refractive index in dependence on temperature and wavelength: a simple approximation," in *Saratov Fall Meeting 2002: Optical Technologies in Biophysics and Medicine IV*, V. V. Tuchin, ed. (International Society for Optics and Photonics, 2003), pp. 393–395.
32. C. A. Volkert and A. M. Minor, "Focused Ion Beam Microscopy and Micromachining," MRS Bull. **32**(05), 389–399 (2007).
33. L. H. Haber, R. D. Schaller, J. C. Johnson, and R. J. Saykally, "Shape control of near-field probes using dynamic meniscus etching," J. Microsc. **214**(1), 27–35 (2004).
34. A. Lazarev, N. Fang, Q. Luo, and X. Zhang, "Formation of fine near-field scanning optical microscopy tips. Part I. By static and dynamic chemical etching," Rev. Sci. Instrum. **74**(8), 3679–3683 (2003).
35. D. B. Leviton and B. J. Frey, "Temperature-dependent absolute refractive index measurements of synthetic fused silica," in *SPIE Astronomical Telescopes + Instrumentation*, E. Atad-Ettedgui, J. Antebi, and D. Lemke, eds. (International Society for Optics and Photonics, 2006), pp. 62732K.

1. Introduction

Optical fiber sensors have been extensively researched and applied for the measurement of many physical, chemical and biological parameters [1]. Two of the most common fiber sensor classifications are intensity- and wavelength-based sensors [2]. While both have application specific advantages, a shift from traditional intensity-based to wavelength-based sensors is clear across the field due to their inherent advantages like independence from power fluctuations, and therefore higher stability. Of these wavelength-based sensors, more specifically the interferometric sensors, a very basic and common structure used in optical

#261196 Received 17 Mar 2016; revised 12 Jun 2016; accepted 12 Jun 2016; published 15 Jun 2016

fiber sensing is the optical cavity, often referred to as a Fabry-Perot interferometer. Such cavities exhibit an interferometric spectrum that results from reflections at the first cavity interface (before the cavity) and a reflection at the second cavity interface (after the cavity). A sensor can be formed as a small change in the cavity length or refractive index can affect the optical path difference between two different light paths. For cavities where the reflectivity is low, such as from a glass-air interface, the system can be approximated by a two wave interferometer:

$$I(\lambda) = I_1(\lambda) + I_2(\lambda) + 2\sqrt{I_1(\lambda) I_2(\lambda)} \cos\left(\frac{2\pi}{\lambda} \cdot OPD + \pi\right) \quad (1)$$

where $I(\lambda)$, $I_1(\lambda)$ and $I_2(\lambda)$ are the total intensity, intensity of path 1 and intensity of path 2 respectively, λ is the free space wavelength, ϕ_0 is the initial phase and OPD is the optical path difference given by:

$$OPD = 2n_{cavity} \cdot l \quad (2)$$

where n_{cavity} and l are the refractive index of the cavity and it's length respectively. Cavities have been realized by creating air bubbles [3,4], depositing metal [5] and dielectric [6,7] films, chemical etching [8], using FBGs as mirrors [9], or even just approaching two cleaved fibers [10]. Micromachining is a more recent technique that allows for the creation of very small cavities or microcavities. The two prominent techniques for optical fiber micromachining are femtosecond laser micromachining [11–17] and focused ion beam (FIB) milling [18–23].

Femtosecond (fs) laser micromachining has been used to create cavities in several ways. Wei *et al.* used a fs-laser to mill an inline cavity and proposed it for temperature [11] and refractive index sensing [12]. Similarly, Ran *et al.* have milled an air-gap and used fringe contrast to develop a temperature-insensitive refractive index sensor [13]. Liao *et al.* have created a bubble-like cavity by drilling a micro-hole on a cleaved fiber facet and then fusion splicing it [14]. They then milled additional side channels to allow the insertion of fluids inside the cavity. Another possibility is to mill a step structure into the end of a cleaved fiber creating a cavity on the fiber top [15]. Equivalent cavities can also be created using focused-ion beam (FIB) micromachining. The advantage of FIB is the superior surface quality of the reflecting surfaces obtained with FIB compared to that produced with a fs-laser [16]. Preliminary work on microcavities milled with FIB has been presented, where cavities have been fabricated in tapered fiber tips for either temperature [18] or refractive index sensing [19,23]. Cavities in microwires for temperature and vibration sensing have been shown [20] as well as focused ion beam milled cavities in polished optical fibers [21]. FIB milling has even been demonstrated in exposed-core suspended core fibers [24].

Among the many known advantages of fiber sensors when compared to more conventional sensors is their ability to simultaneously measure more than one parameter. This is particularly useful when considering refractive index and temperature. Simultaneous measurement of refractive index and temperature was successfully achieved using FBGs [25,26], long period gratings [27], hybrid FBG/LPG gratings [28], among others. Interferometers can also be used but their serial multiplexing is limited by their complex spectra. These spectra are formed by the sum of the contributions of each pair of interfering waves. Nevertheless, two parameter sensing using interferometers has been achieved both with a Mach-Zehnder [29] and a Fabry-Perot interferometers [30].

When using two sensors in series the physical separation between the two sensing elements can lead to a mismatch when it comes to temperature compensation [31], especially when considering very small volumes or radical changes in temperature. Nguyen *et al.* have created a Fabry-Perot structure for temperature and salinity sensing but in standard SMF

#261196 Received 17 Mar 2016; revised 12 Jun 2016; accepted 12 Jun 2016; published 15 Jun 2016

which does not have the tapered fiber tip profile and advantages of the structures proposed in this work [22].

In this work, we demonstrate simultaneous measurement of temperature and refractive index using focused ion beam milled Fabry-Perot cavities in optical fiber micro-tips. We examine the sensing characteristics of these sensors by fabricating two different cavity designs milled in tapered fiber tips (TFTs). The first cavity is a milled portion of the fiber tip exposing it to the external refractive index and the second cavity is created by milling two thin slots into the TFT effectively creating two mirrors that form a solid silica cavity. These cavities are found to have different responses to temperature and refractive index leading to a third type of structure. Here, a solid silica cavity and a gap cavity are combined to form a complex structure. This structure presents a spectrum with three different cavities. The cavities are further processed and demultiplexed in the Fourier domain, allowing the simultaneous measurement of temperature and refractive index.

2. FIB milling of tapered fiber tips

Focused ion beam, much like its electron beam sibling, uses a set of electromagnetic lenses to focus a beam of ions on the surface of a sample. Unlike the electrons used in scanning electron microscopy (SEM), the ions not only have a much larger mass (approximately 130000 times larger for Ga^{+}) but also a larger size (approximately 20000 times) and thus will eject material from the surface on which they are focused. Besides the sample material properties such as atomic number/density and chemical bonding, the milling rate depends on several beam parameters such as ion beam current, beam energy and incidence angle [32]. Using this milling characteristic of the FIB technology, a myriad of structures can be created on any type of material.

FIB was used to mill different types of cavity structures on tapered optical fiber tips. The tapered fiber tips (TFTs) were fabricated using dynamic chemical etching [33]. This technique allows the fine control of the TFT length and cone angle. Different from traditional dynamic chemical etching where the fiber is moved relative to the meniscus position [34], here a syringe pump is used to control the relative position of etchant and fiber. The syringe pump changes the amount of acid in the container and changes the surface level and then, changes the length of the fiber dipped in the acid. All the fibers used to create tips were single mode fibers (SMF-28).

The Fabry-Perot cavities were milled using a dual beam FIB-SEM TESCAN system (Lyra XMU). The system is equipped with a liquid metal ion source (LMIS) for generating a focused beam of gallium ions. For FIB milling, a conductive sample is desirable to avoid charge accumulation on the surface and subsequent beam deviation. As glass optical fibers are electrically insulating, other measures are implemented to avoid these problems. The fiber tips were first mounted and glued onto an aluminum block using a silver paste. A thin metallic film (50 nm of tantalum) was then sputtered onto the TFT in order to ensure a sufficient surface conductivity. The milling was performed with a high initial current (1-3 nA) to roughly mill the cavities, and then a lower current (200-400 pA) was used to polish the mirror surfaces in order to have a smoother reflecting surface. The energy of the incident ions was set to 30 keV in all cases.

3. Air-gap and double slot cavities

3.1. FIB milling of the cavities

Two different Fabry-Perot cavities were milled in TFTs: (1) an air-gap with an approximate length of 53 μm was milled into the TFT, and (2) two thin slots (ca. 2 μm) were milled with a spacing of 50 μm creating a solid silica cavity [Fig. 1]. The objective is to create and compare two similarly sized cavities but one in air and the other in silica. The two structures were fabricated in two steps: first, the main structure, such as the air-gap and the slots, was created

#261196 Received 17 Mar 2016; revised 12 Jun 2016; accepted 12 Jun 2016; published 15 Jun 2016

and then the tip was sharpened to reduce reflections. FIB was used to mill the very tip of the structures into a sharp pointy tip to avoid back reflections.

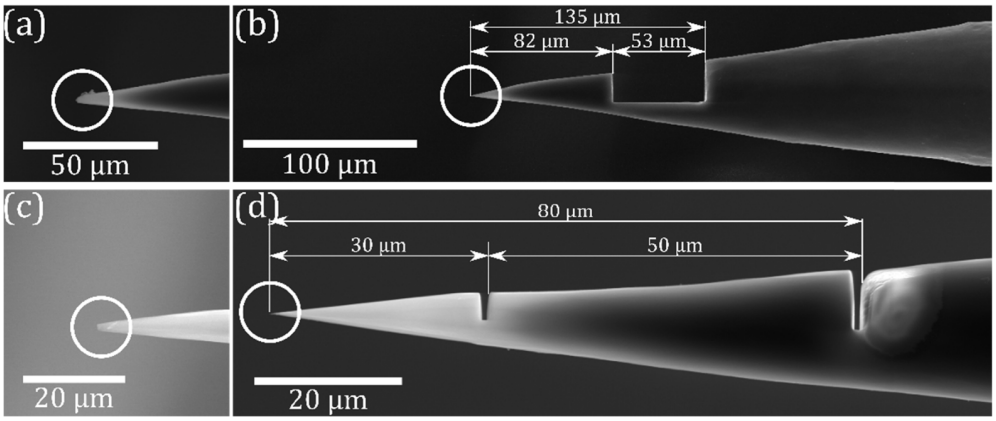

Fig. 1. SEM micrographs of both Fabry-Perot cavities milled in TFTs: air-gap cavity before (a) and after sharpening (b), and double-slot silica cavity before (c) and after sharpening (d).

3.2. Optical characterization

The milled structures shown in Fig. 1 were spectrally analyzed using a simple reflection setup with a supercontinuum source (Fianium WL-SC-400-2), an optical circulator, and an optical spectrum analyzer (ANDO AQ6315), before and after sharpening the tip.

The spectra before [Fig. 2(a)] and after [Fig. 2(b)] sharpening and the respective fast Fourier transforms (FFTs) [Fig. 2(c) and 2(d)] for the air-gap structure are shown. Before performing the FFTs, the wavelength data was converted to optical frequency because the free spectral range is uniform in optical frequency but not in wavelength, where it depends on the square of the wavelength [24].

Before sharpening, three different cavities are visible, either in the complex spectrum or by the three peaks visible in the FFT. The first peak, seen in both graphs in Fig. 2, relates to the 53 µm-long air-gap [see Fig. 3(a)]. The second peak (82 µm × 1.444 ≈118 µm) is the silica cavity between the second interface and the tip, and the third peak (82 µm × 1.444 + 53 µm ≈171 µm) is from the first interface and the tip. After sharpening, the reflection at the tip disappears and with it the two cavities relying on this mirror also disappear, leaving a clean spectrum [Fig. 2(b)] with a sole peak in the Fourier transform [Fig. 2(d)]. Sharpening the tip effectively eliminates the inherent reflection caused by an imperfect or broken tip [Fig. 3].

#261196 Received 17 Mar 2016; revised 12 Jun 2016; accepted 12 Jun 2016; published 15 Jun 2016

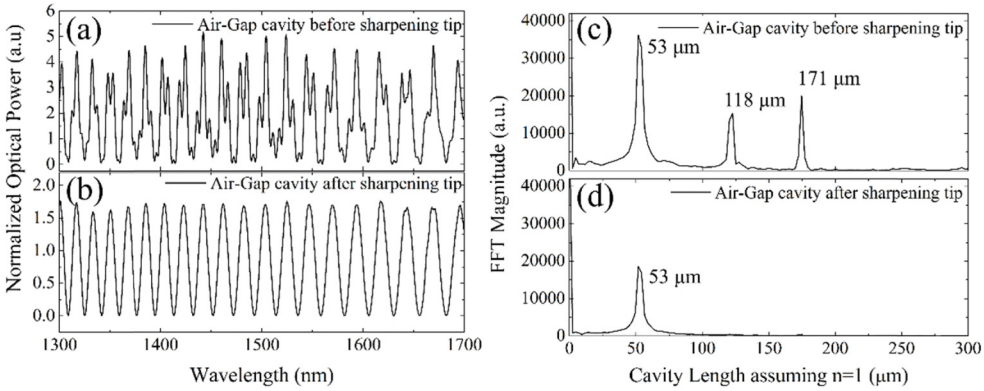

Fig. 2. Spectral analysis of the air-gap cavity. Shown is the air-gap spectrum (a) before sharpening the tip and (b) after sharpening the tip. The optical power is normalized to the reflected power at a cleaved SMF. (c) and (d) show the respective FFTs considering a cavity refractive index of 1.

Estimating the losses of such a structure, from Eq. (1) one should have a maximum of 4 times the reflectivity of a cleaved glass-air interface assuming the reflected intensity from each interface is the same. Looking at Fig. 2(b), one has almost half of that. This amounts to a 3 dB loss due to cavity imperfections from FIB milling (surface angle, surface roughness), the Ta-film, and taper losses.

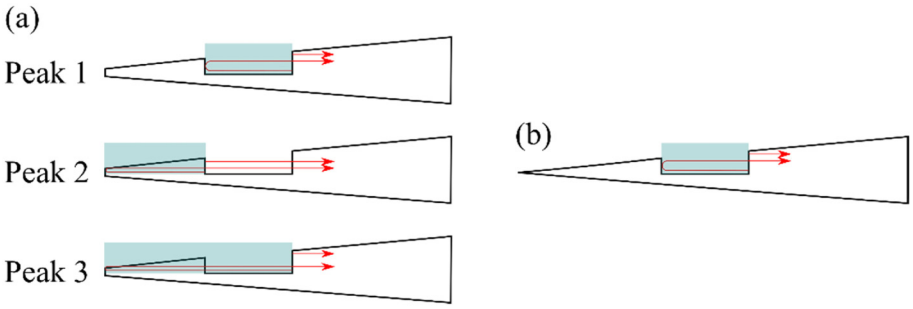

Fig. 3. Schematics of the cavities related to each peak present in the FFT spectra of the air-gap cavity (a) before the tip is sharpened and (b) after the tip is sharpened.

For the double-slot silica cavity [Fig. 1(d)], three peaks are present before sharpening, due to the three cavities, mostly in silica, between the first and second slot and the tip [Fig. 4(c)]. These cavities are shown schematically in Fig. 5. After sharpening the tip, only the cavity between the two slots remains, shown by the sole peak in the FFT [Fig. 4(d)]. The spectrum from the sharpened structure [Fig. 4(b)] shows a low frequency component, indicated by the low visibility at longer wavelengths. This is a result of the 2 µm-long slots. The peaks are not present in the Fourier transform [Fig. 4(d)] as the length is too small and is masked by the peak at 0 cavity length.

#261196 Received 17 Mar 2016; revised 12 Jun 2016; accepted 12 Jun 2016; published 15 Jun 2016

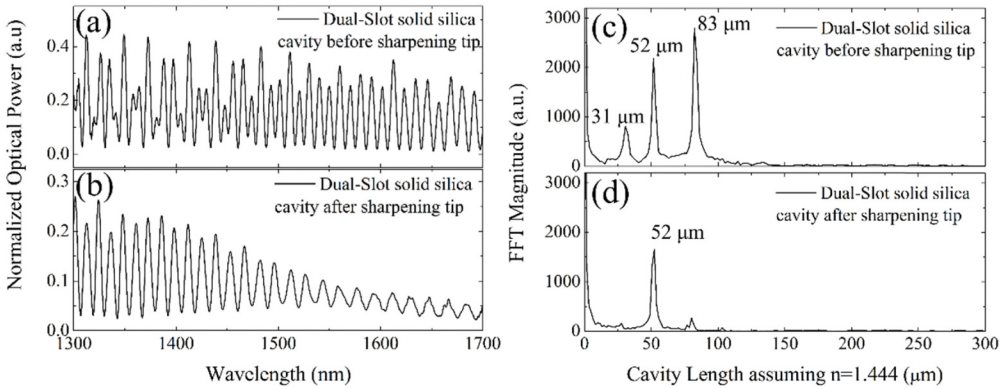

Fig. 4. Spectral analysis of the dual-slot cavity. Shown is the dual-slot spectrum (a) before sharpening the tip and (b) after sharpening the tip. The optical power is normalized to the reflected power at a cleaved SMF. (c) and (d) show the respective FFTs considering a cavity refractive index of 1.444.

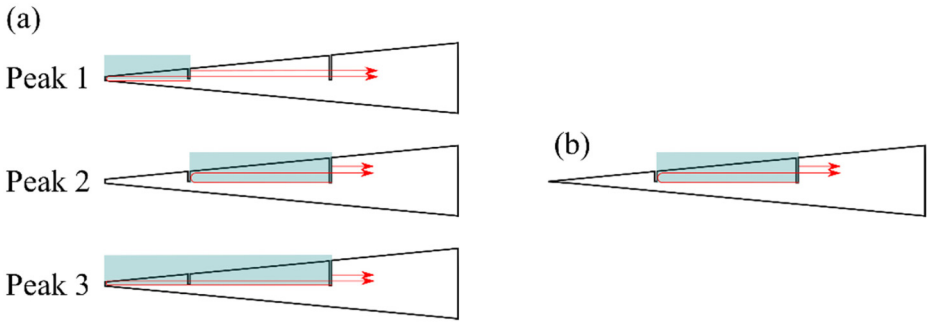

Fig. 5. Schematics of the cavities related to each peak present in the FFT spectra of the double-slot cavity (a) before the tip is sharpened and (b) after the tip is sharpened.

3.3. Temperature characterization

Analyzing both structures' response to temperature variations between 300 °C and 1000 °C, two very different responses are obtained [Fig. 6]. The double slot cavity is relatively more temperature sensitive (17.9 pm/K) compared to the air gap cavity, which is essentially insensitive to temperature (0.17 pm/K). The reason behind this difference is readily perceived from the analysis of the cavity structures. The double slot cavity is a silica cavity and thus the sensitivity can be given by:

$$\Delta\lambda_0 = \lambda_0 \left(\alpha_{TO}^{Silica} + \alpha_{TE}^{Silica} \right) \Delta T \tag{3}$$

where α_{TO}^{Silica} is the thermo-optic coefficient of silica (8.6×10^{-6} K^{-1}) [35] and α_{TE}^{Silica} is the coefficient of thermal expansion of silica (0.55×10^{-6} K^{-1}) [14]. This means that the main contribution to the thermal sensitivity is due to the change in refractive index of silica with temperature. On the other hand, for the air-gap structure, sensitivity can be described as follows:

$$\Delta\lambda_0 = \lambda_0 \left(\alpha_{TO}^{Air} + \alpha_{TE}^{Silica} \right) \Delta T \tag{4}$$

where α_{TO} is the thermo-optic coefficient of air (-0.9×10^{-6} K^{-1}) and α_{TE} is the coefficient of thermal expansion of silica (0.55×10^{-6} K^{-1}). The thermo-optic coefficient of air is not only one order of magnitude smaller than that of silica, but also of opposite sign. Here, the thermo-

#261196 Received 17 Mar 2016; revised 12 Jun 2016; accepted 12 Jun 2016; published 15 Jun 2016

optic coefficient of air is employed because light travels through the air gap yet expansion still occurs in the silica below the air gap. Theoretically, this would lead to sensitivities of 14.2 pm/K at 1550 nm for the double-slot silica cavity and −0.54 pm/K for the air-gap cavity. The double-slot cavity sensitivity is similar to the predicted one (predicted value: 13.7 pm/K vs. measured value: 17.9 pm/K) and for the air-gap cavity, both predicted and calculated sensitivities are negligible (predicted value: −0.54 pm/K vs. measured value: 0.17 pm/K).

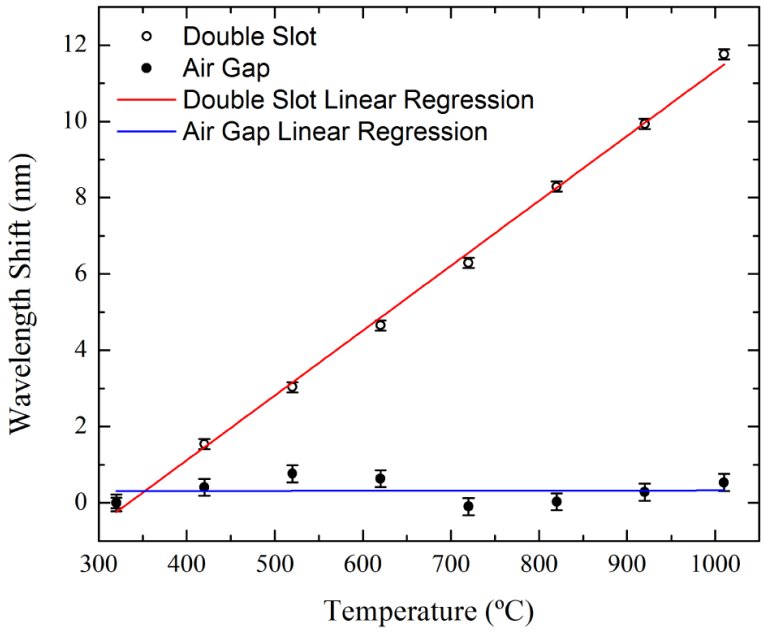

Fig. 6. Temperature characterization of both structures: double-slot solid silica (O-red) and air-gap (●-blue) cavities. The solid silica cavity and air gap cavity sensitivities are 17.9 pm/K and 0.17 pm/K respectively.

To study the response of the cavities to changes in the refractive index of the surrounding medium, both the air-gap structure and the double-slot structure were dipped in ethanol. In Fig. 7, the FFTs of the spectra in air and in ethanol are compared. For the air-gap cavity, the FFT peak that initially presents itself at 53 μm shifts to 72 μm (53 μm × 1.352≈71.7 μm) due to the fact that the cavity is no longer filled with air but with ethanol. For the double-slot structure, the FFT peak does not shift when dipped in ethanol. This occurs because the cavity is entirely in silica and dipping the tip in ethanol will not change the refractive index of the cavity. One other consequence of dipping the tips in ethanol is that the magnitude of the FFT peak decreases by approximately 16 times. This results from the fact that the refractive index difference when the structures are dipped in ethanol becomes much smaller and consequently the reflectivity at each interface decreases.

#261196 Received 17 Mar 2016; revised 12 Jun 2016; accepted 12 Jun 2016; published 15 Jun 2016

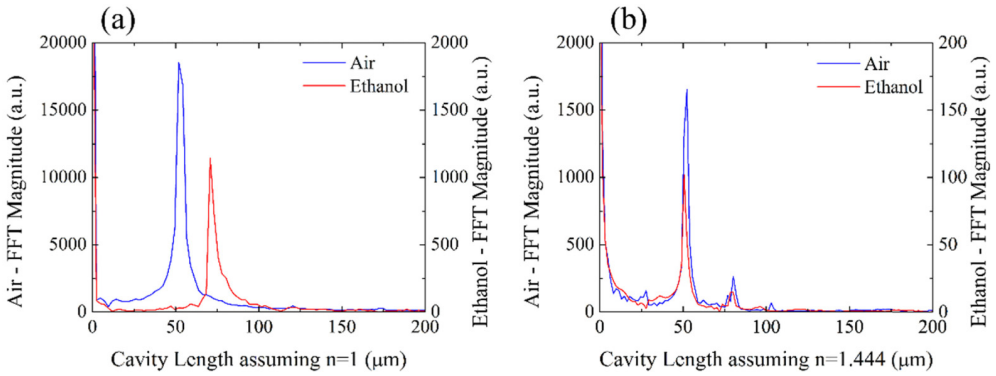

Fig. 7. FFTs of the spectra of the (a) air-gap cavity and (b) double-slot cavity when in air or dipped in ethanol.

These very different responses to temperature and external refractive index from both types of cavities can be explored by performing simultaneous measurement of temperature and other parameters. While a silica cavity is essentially only sensitive to temperature, the air-gap cavity can be used for simple refractive index sensing or could be chemically functionalized for performing bio-assays.

4. Dual-cavity structure

4.1. Fabrication and optical characterization

A structure can be created incorporating both concepts of air-gap cavity and solid silica cavity. Such a dual-cavity is shown in Fig. 8. where an air-gap cavity was milled in a sharp-pointed TFT. In Fig. 8(b), that sharp tip was then milled off and polished creating an intentional additional reflecting surface. This results in two sections, one 55 μm-long in air and one 65 μm-long in silica.

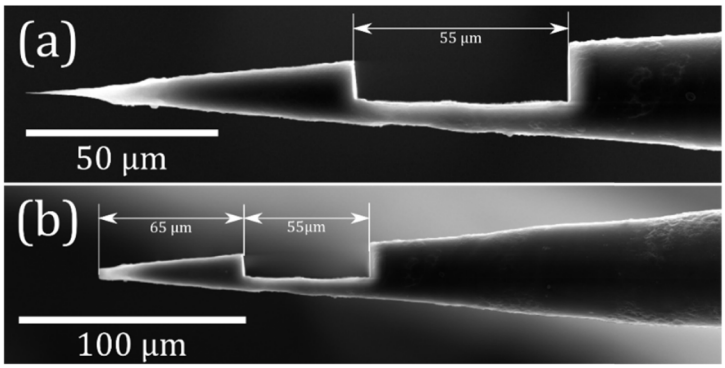

Fig. 8. SEM micrograph of the dual-cavity structure: (a) before creating the silica cavity in the tip and (b) after polishing the tip into a reflecting surface.

Looking at the Fast Fourier Transforms of the spectra of both these structures when in air (n = 1.000) or immersed in isopropanol (n = 1.373) several peaks can be observed [see Fig. 9(a,b)]. In this case, the FFTs are represented in terms of overall optical path difference because the light path towards the tip is not always the same when light comes back. The first peak at 110 μm in air (2 × 55 μm × 1.000) and at 151 μm in isopropanol (2 × 55 μm × 1.373) originates in the milled cavity. This peak shifts due to the change in refractive index when the tip is immersed in isopropanol (151-110 = 41 μm). The exact same shift occurs for the third

#261196 Received 17 Mar 2016; revised 12 Jun 2016; accepted 12 Jun 2016; published 15 Jun 2016

peak in air at 297.8 μm [2 × (55 μm × 1.000 + 65 μm × 1.444)]; leading to a peak at 338.6 μm [2 × (55 μm × 1.373 + 65 μm × 1.444)] in isopropanol.

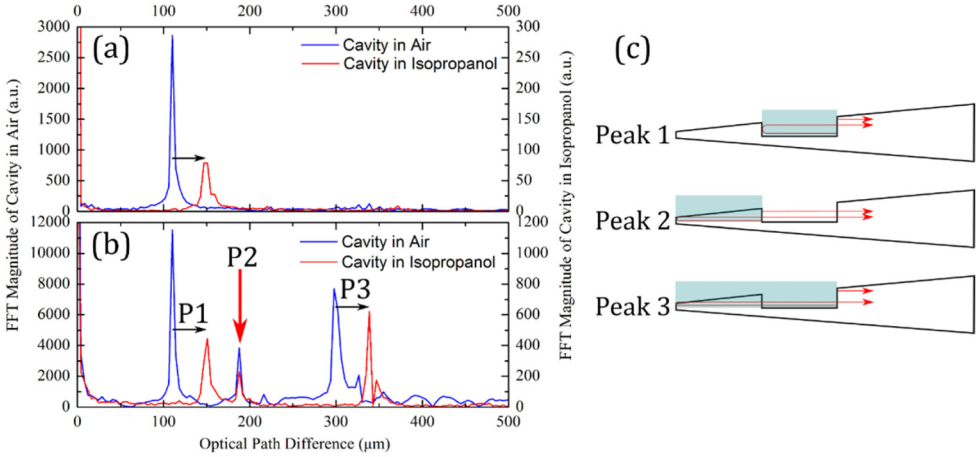

Fig. 9. Fast Fourier transforms of the spectra from the dual cavity structure (a) before polishing the tip into a mirror and (b) after polishing and creating the final structure; (c) schematic of the cavity related to each FFT peak.

However, the second peak, at 187.7 μm (2 × 65 μm × 1.444), does not shift when immersed in isopropanol because this cavity is entirely in silica. From this, one can deduce that two of the cavities (FFT peaks 1 and 2) that are present, are independent or almost independent when it comes to temperature and refractive index. A third cavity (FFT peak 3) is the sum of the other two cavities, thus being responsive to temperature and refractive index of the surrounding medium.

4.2. Temperature and refractive index characterization

To demonstrate simultaneous measurement of temperature and refractive index we performed measurements with variations of temperature in air and in water. The use of water here was due to the higher relevance of water when compared to isopropanol for potential applications in biosensing. To fully understand the response of each cavity individually a processing of the spectral signals was necessary. First, a fast Fourier transform of the original spectrum was performed. A band pass filter was then applied, where each individual FFT peak was filtered and the signal of each was then converted back into wavelength. With these clean spectra from each FFT peak, the spectral shift was monitored when temperature changes were applied.

In Fig. 10, the shifts of the reconstructed spectra for each FFT peak are shown when the surrounding air temperature is changed from 40 °C to 140 °C. Peak 1, that corresponds to the air-gap cavity has a very low sensitivity (–0.4 pm/K) as expected because, just like the air-gap cavity in section 3, this cavity's sensitivity is given by Eq. (4). Peak 2, corresponding to an all silica cavity, similar to the double-slot cavity of section 3, has a sensitivity of –15.8 pm/K. Peak 3, that derives from a cavity that encompasses both of the previous ones results in an intermediate sensitivity of –9.6 pm/K. It is possible to compare this value with a value obtained from the weighted average of the other two sensitivities. Using Eq. (5), derived from the accumulated phase difference, one can estimate the sensitivity of the peak 3 cavity to be -10.1 pm/K [see Eq. (6)], which is in accordance with the value experimentally calculated.

$$\left(\frac{d\lambda}{dT}\right)_{\text{Peak3}} = \frac{OPD_{\text{Peak1}}}{OPD_{\text{Total}}}\left(\frac{d\lambda}{dT}\right)_{\text{Peak1}} + \frac{OPD_{\text{Peak2}}}{OPD_{\text{Total}}}\left(\frac{d\lambda}{dT}\right)_{\text{Peak2}} \quad (5)$$

#261196 Received 17 Mar 2016; revised 12 Jun 2016; accepted 12 Jun 2016; published 15 Jun 2016

$$\left(\frac{d\lambda}{dT}\right)_{\text{Peak 3}}^{\text{Estimated}} = \frac{55\,\mu\text{m}\times 1.0}{55\,\mu\text{m}\times 1.0+65\,\mu\text{m}\times 1.444}(-0.4\,\text{pm/K})+ \\ +\frac{65\,\mu\text{m}\times 1.444}{55\,\mu\text{m}\times 1.0+65\,\mu\text{m}\times 1.444}(-15.8\,\text{pm/K}) \\ =-10.1\,\text{pm/K} \tag{6}$$

This shows that the response of the large cavity (FFT peak 3) is the sum of the responses of each of the two smaller cavities (FFT peaks 1 and 2), as expected (estimated sensitivity: -10.1 pm/K vs. measured sensitivity: –9.6 pm/K).

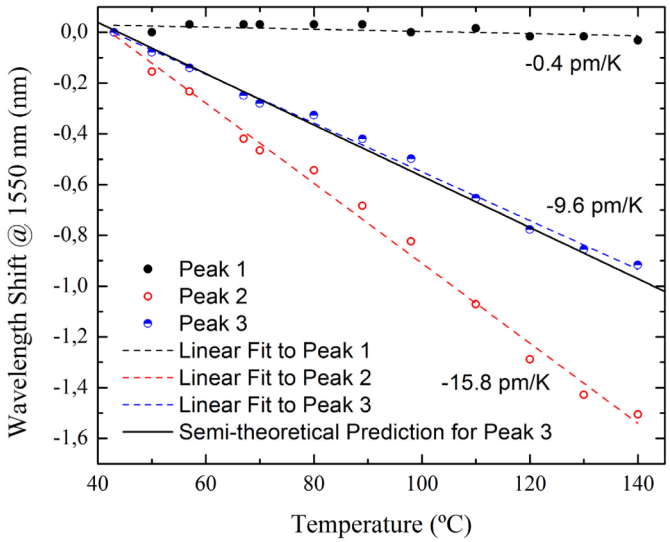

Fig. 10. Temperature characterization of the dual cavity structure when in air.

The same temperature analysis was performed in water: the same sensor was dipped in water whose temperature was changed between 25°C and 95°C [Fig. 11]. A similar situation occurs but now the gap cavity is filled with water, which has a very different thermo-optic coefficient. The index variation of water with temperature is non-linear, which leads to data in Fig. 11 that is clearly non-linear for the peaks that include the water cavity (Peak 1 and Peak 3). Since the thermo-optic coefficient of water is much higher than that of air and silica, the shifts of the spectra related to the water cavity are now much larger than those of the silica cavity. This explains the much higher sensitivity of spectra related to FFT Peak 1.

#261196 Received 17 Mar 2016; revised 12 Jun 2016; accepted 12 Jun 2016; published 15 Jun 2016

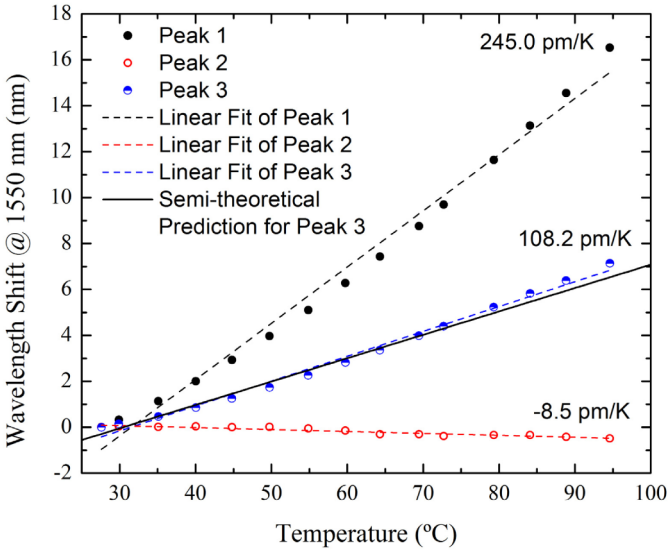

Fig. 11. Temperature characterization of the dual cavity structure when immersed in water.

This temperature sensitivity presented as is, is only valid in water but knowing the thermal variation of the index of refraction of water allows the determination of the refractive index sensitivity of this cavity [31]. Subtracting the almost negligible contribution of the thermal expansion of silica and converting the temperature of water into the respective refractive index, one can obtain the values shown in Fig. 12. Performing a linear fit of the data, a sensitivity of - 1316 nm/RIU is obtained with a coefficient of determination $R^2 = 0.9998$.

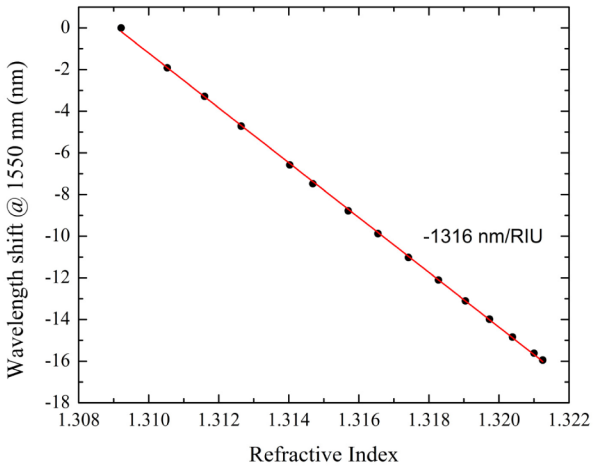

Fig. 12. Refractive index characterization in the range [1.309 - 1.321].

The sensitivity of a Fabry-Perot cavity should be equal to λ/n, which can be derived from Eq. (1). This is approximately 1180 nm/RIU at a wavelength of 1550 nm and a refractive index of 1.318 (water at 1550 nm). This is generally in agreement with experimentally observed results in the literature (see Table 1), and is close to the measured sensitivity in our work. Furthermore, measurements to determine the minimum detection limit were performed. The spectral variation during 1 hour was recorded with the structure immersed in water. This lead to variations of ± 0.67 nm (considering three standard variations) which in turn leads to a refractive index detection limit of 5.1×10^{-4} RIU for a single spectral scan.

#261196 Received 17 Mar 2016; revised 12 Jun 2016; accepted 12 Jun 2016; published 15 Jun 2016

Table 1. Comparison of Fabry-Perot cavity sensitivities milled with FIB and femtosecond laser

Year	*Configuration*	*Sensitivity @ 1550 nm*
2008 [12]	fs-laser-milled cavity in standard-diameter SMF	1163 nm/RIU @ 1.33
2011 [19]	FIB-milled cavity in a 32-μm tapered fiber	1731 nm/RIU @ 1.3
2012 [14]	fs-laser-milled microchannel in SMF	994 nm/RIU @ 1.31-1.39
This Work	FIB-milled cavity in tapered fiber tip	1316 nm/RIU @ 1.309-1.321

This results in a structure with two physical cavities, one where the influence of temperature is negligible (and easily compensated), but the refractive index can be measured, and one sensitive to temperature changes where refractive index changes in the external medium have little effect. Taking this into account and performing the appropriate calibration it is possible to use two different FFT peaks (corresponding to two different cavities) as they have such distinct responses. These structures are can be reproduced within the resolution limits of the focused-ion beam milling process (less than 100 nm), allowing sensors with nominally the same properties to be obtained. While there are subtle variations in the spectrum between samples, Fourier analysis techniques allow the optical path length of the cavity to be extracted from the spectrum and the sensitivity to temperature and refractive index can be calibrated from this.

5. Conclusion

In this work, several types of cavities have been milled in tapered fiber tips using focused ion beam technology. Cavities in silica, insensitive to the external medium's refractive index have been shown, as well as gap cavities that are insensitive to temperature yet present sensitivity to the surrounding refractive index. Both cavity types have been combined to create a structure that can be used to measure temperature and refractive index independently. These structures have been fabricated with a total length of 110 μm and a maximum diameter of 25 μm, at the start of the sensing structure, allowing for measurements at micron-scaled dimensions. These structures showed spectra where three interferometers are present resulting from three cavities formed by the top and the mirror surfaces of the gap. These three cavities present distinct sensitivities to temperature and refractive index, with respective sensitivities of −15.8 pm/K and −1316 nm/RIU.

Acknowledgments

Project "Coral - Sustainable Ocean Exploitation: Tools and Sensors/NORTE-01-0145-FEDER-000036" is financed by the North Portugal Regional Operational Programme (NORTE 2020), under the PORTUGAL 2020 Partnership Agreement, and through the European Regional Development Fund (ERDF). Ricardo André is supported by Fundação para a Ciência e a Tecnologia through the grant SFRH/BD/84048/2012. Stephen Warren-Smith is funded by the European Commission through the Seventh Framework Programme (FP7), PIIF-GA-2013-623248.